Thermal Unfolding of Unsolvated Cytochrome *c*: Experiment and Molecular Dynamics Simulations

Yi Mao, Jürgen Woenckhaus, Jiri Kolafa,† Mark A. Ratner,* and Martin F. Jarrold*

Contribution from the Department of Chemistry, Northwestern University, 2145 Sheridan Road, Evanston, Illinois 60208

Received January 28, 1998

Abstract: The thermal unfolding of unsolvated cytochrome *c* has been examined in the gas phase using ion-mobility measurements. Measurements were performed for the +5, +6, and +7 protonated charge states from around room temperature up to 573 K. The $(M + 5H)^{5+}$ charge state remains folded at 573 K while $(M + 6H)^{6+}$ and $(M + 7H)^{7+}$ go through a series of unfolding transitions as the temperature is raised. Molecular dynamics simulations were performed using the CHARMM force field. The simulations are in qualitative agreement with the experimental results: the +7 charge states unfold as the temperature is raised and the +5 charge states remain compact. Addition of two protons to the +5 charge state flattens the energy landscape so that the folded and unfolded conformations have similar energies. Entropy presumably drives the unfolding of the +7 charge state as the temperature is raised.

I. Introduction

Protein structure and folding are controlled by intramolecular interactions and hydration effects. While the folding free energy of a protein in solution is typically tens of kilojoules per mole at room temperature, protein intramolecular interactions and hydration energies are both estimated to be several thousand kilojoules per mole for a small protein.[1,2] Thus, the small folding free energy in solution results from the near cancellation of several much larger contributions. It is difficult to obtain information about the individual contributions from solution studies. However, in the gas phase, hydration effects vanish, and this environment can provide important information about intramolecular interactions within proteins. Several groups have begun to examine the conformations of unsolvated peptides and proteins in the gas phase, using a variety of techniques.[3−19] We have reported studies of BPTI, cytochrome *c*, and apomyoglobin using ion-mobility measurements.[20−23] The mobility of a gas-phase ion depends on its collision cross section, so ion-mobility measurements can resolve different conformations and can be used to obtain tertiary structure information about unsolvated proteins.

For cytochrome *c*, our measurements have shown that there is a sharp unfolding transition between the $(M + 5H)^{5+}$ and $(M + 7H)^{7+}$ charge states.[22] The unfolding transition is believed to be caused by Coulomb repulsion, and it is somewhat analogous to acid denaturation in solution. In this paper, we present the results of more detailed studies of this unfolding transition. Ion mobility measurements show that the +5 charge state remains compact even at 573 K, while the +6 and +7 charge states undergo a series of unfolding steps as the temperature is raised. These experimental results are compared to molecular dynamics (MD) simulations with the CHARMM force field.[24,25] Such a comparison provides information about the reliability of the MD simulations, and, if the simulations are in agreement with experiment, the combination can be used to derive insight that is not available from the experiments alone.

* To whom correspondence should be addressed. MAR Tel.: (847) 491-5652. Fax: (847) 491-7713. E-mail: ratner@mercury.chem.nwu.edu. MFJ Tel.: (847) 491-7553. Fax: (847) 491-7713. E-mail: mfj@nwu.edu.

† Permanent address: E. Hala Laboratory of Thermodynamics, Institute of Chemical Process Fundamentals, 16502 Praha 6-Suchdol, Czech Republic.

(1) Lazaridis, T.; Archontis, G.; Karplus, M. *Adv. Protein Chem.* **1995**, *47*, 307.
(2) Makhatadze, G. I.; Privalov, P. *Adv. Protein Chem.* **1995**, *47*, 231.
(3) Winger, B. E.; Light-Wahl, K. J.; Rockwood, A. L.; Smith, R. D. *J. Am. Chem. Soc.* **1992**, *114*, 5897.
(4) Suckau, D.; Shi, Y.; Beu, S. C.; Senko, M. W.; Quinn, J. P.; Wampler, F. M.; McLafferty, F. W. *Proc. Natl. Acad. Sci. U.S.A.* **1993**, *90*, 790. Wood, T. D.; Chorush, R. A.; Wampler, F. M.; Little, D. P.; O'Connor, P. B.; McLafferty, F. W. *Proc. Natl. Acad. Sci. U.S.A.* **1995**, *92*, 2451.
(5) McLafferty, F. W.; Guan, Z.; Haupts, U.; Wood, T. D.; Kelleher, W. L. *J. Am. Chem. Soc.* **1998**, *120*, 4732.
(6) Covey, T. R.; Douglas, D. J. *J. Am. Soc. Mass Spectrom.* **1993**, *4*, 616.
(7) Douglas, D. J. *J. Am. Soc. Mass Spectrom.* **1994**, *5*, 17.
(8) Collings, B. A.; Douglas, D. J. *J. Am. Chem. Soc.* **1996**, *11*, 4488.
(9) Cox, K. A.; Julian, R. K.; Cooks, R. G.; Kaiser, R. E. *J. Am. Soc. Mass Spectrom.* **1994**, *5*, 127.
(10) Reimann, C. T.; Quist, A. P.; Kopniczky, J.; Sundqvist, B. U. R.; Erlandsson, R.; Tengvall, P. *Nucl. Instrum. Methods Phys. Res., Sect. B* **1994**, *88*, 29.
(11) Quist, A. P.; Ahlbom, J.; Reimann, C. T.; Sundqvist, B. U. R. *Nucl. Instrum. Methods Phys. Res., Sect. B* **1994**, *88*, 164.
(12) Sullivan, P. A.; Axelsson, J.; Altman, S.; Quist, A. P.; Sundqvist, B. U. R.; Reimann, C. T. *J. Mass Spectrom.* **1995**, *7*, 329.
(13) Gross, D. S.; Schnier, P. D.; Rodriguez-Cruz, S. E.; Fagerquist, C. K.; Williams, E. R. *Proc. Natl. Acad. Sci. U.S.A.* **1996**, *93*, 3143.
(14) Von Helden, G.; Wyttenbach, T.; Bowers, M. T. *Science* **1995**, *267*, 1483.
(15) Wyttenbach, T.; Von Helden, G.; Bowers, M. T. *J. Am. Chem. Soc.* **1996**, *118*, 8355.
(16) Cassady, C. J.; Carr, S. R. *J. Mass Spectrom.* **1996**, *31*, 247.
(17) Camara, E.; Green, M. K.; Penn, S. G.; Lebrilla, C. B. *J. Am. Chem. Soc.* **1996**, *118*, 8751.
(18) Valentine, S. J.; Clemmer, D. E. *J. Phys. Chem. B* **1997**, *101*, 3891.
(19) Valentine, S. J.; Clemmer, D. E. *J. Am. Chem. Soc.* **1997**, *119*, 3558.
(20) Clemmer, D. E.; Hudgins, R. R.; Jarrold, M. F. *J. Am. Chem. Soc.* **1995**, *117*, 10141.
(21) Shelimov, K. B.; Jarrold, J. F. *J. Am. Chem. Soc.* **1996**, *118*, 10313.
(22) Shelimov, K. B.; Clemmer, D. F.; Jarrold, M. F. *J. Am. Chem. Soc.* **1997**, *119*, 2240.
(23) Shelimov, K. B.; Jarrold, M. F. *J. Am. Chem. Soc.* **1997**, *119*, 2987.
(24) Brooks, B. R.; Bruccoleri, R. E.; Olafson, B. D.; States, D. J.; Swaminathan, S.; Karplus, M. *J. Comput. Chem.* **1983**, *4*, 187.

10.1021/ja980324b CCC: $18.00
Published on Web 03/11/1999

In the present case, the simulations are in qualitative (but not quantitative) agreement with the experimental results. We discuss the origins of the lack of quantitative agreement. The simulations, nevertheless, provide important insight into the key features of the experimental results.

II. Experimental Methods

The injected ion drift tube apparatus and electrospray source have been described previously.[22] Bovine or equine cytochrome *c* (Sigma Chemical Co.) at around 5×10^{-4} M in a 3:1 mixture of water and acetonitrile was electrosprayed in air. The ions enter the apparatus through a 0.012 cm diameter aperture into a desolvation region. After passing through the desolvation region (kept at 300 K) the ions are carried into the source vacuum chamber and focused into a quadrupole mass spectrometer. At the end of the quadrupole, the ions are focused and injected into a drift tube. The drift tube was operated with a helium buffer-gas pressure of 5−8 Torr and with a drift field of 13.16 V/cm. The drift tube was heated by cartridge heaters inserted into its walls, and the temperature was monitored by five thermocouples and regulated to within ±1 K. After traveling through the drift tube, the ions that exit are focused into a second quadrupole mass spectrometer and then detected by an off-axis collision dynode and dual microchannel plates. Ion mobilities were measured by injecting 50-μs pulses of ions into the drift tube and recording their arrival-time distributions at the detector using a multichannel scaler. Drift-time distributions were obtained from the arrival-time distributions by correcting the time scale so that it only reflects the amount of time spent traveling across the drift tube. The reduced mobility, K_o, is related to the drift time, t_D, by

$$K_o = \frac{L}{t_D E}\frac{273.15}{T}\frac{P}{760} \tag{1}$$

where E is the electric field in the drift tube, T is the buffer-gas temperature, P is the buffer-gas pressure, and L is the length of the drift tube. The measured mobilities can be converted into average collision cross sections using[26]

$$\Omega_{avg}^{(1,1)} = \frac{(18\pi)^{1/2}}{16}\left[\frac{1}{m}+\frac{1}{m_b}\right]^{1/2}\frac{ze}{(k_B T)^{1/2}}\frac{1}{K_o}\frac{1}{\rho} \tag{2}$$

In this expression, m is the mass of the ion, m_b is the mass of a buffer gas atom, ze is the charge on the ion, and ρ is the buffer-gas number density at STP.

III. Cross Section Calculations

Structural information is obtained from ion-mobility measurements by comparing the measured cross sections to cross sections calculated for geometries derived from theoretical studies. The average cross section, $\Omega_{avg}^{(1,1)}$, in eq 2 above is really an orientationally averaged collision integral which should be calculated by averaging the momentum-transfer cross section over relative velocity and collision geometry. The momentum-transfer cross section is obtained by averaging a function of the scattering angle over the impact parameter.

Table 1 shows collision integrals calculated using the classical trajectory method[27] for neutral equine cytochrome *c* (crystal-structure coordinates)[28] at several different temperatures. These calculations were performed using an effective protein-buffer gas potential given by the sum of two body Lennard-Jones interactions.[27,29] Trajectories are averaged until the collision integral converges. In this case, 40 000−50 000 trajectories were averaged, and the standard error of the mean is around 1%. As the temperature is raised, there is a small decrease, around 4%, in the collision integral. This decrease can be attributed to (1) the long-range, attractive part of the intermolecular potential between a buffer gas atom and the protein becoming less important as the temperature is raised and (2) trajectories traveling further up the repulsive part of the potential at the higher temperature. These results indicate that changes of greater than a few percentage points in the collision integrals measured in the 300−600 K temperature range must be due to conformational changes.

Table 1. Collision Integrals Calculated for Neutral Equine Cytochrome *c* Using the Trajectory Method[a]

temperature, K	collision integral, Å^2
298	1334
400	1297
500	1299
600	1284

Calculating collision integrals for a protein the size of cytochrome *c* by the trajectory method uses a lot of computer time. Thus, in the MD simulations described below, where cross sections must be determined for a large number of conformations, we used the exact hard spheres scattering model.[30] Cross sections calculated for the native conformation with this model are within 1% of those determined by the trajectory method. To account for the small temperature dependence in the cross sections calculated for the native conformation using the trajectory method, the hard sphere contact distances used in the exact hard spheres scattering model were scaled to reproduce the cross sections calculated using the trajectory method.

IV. Experimental Results

The most convenient way to display drift-time distributions recorded at different temperatures is to convert to a collision cross section scale using equations 1 and 2 above. Figure 1 shows cross section distributions obtained for the $(M + 5H)^{5+}$ charge states of bovine cytochrome *c*, from around 273 K up to around 573 K. The near-vertical dashed line in Figure 1 shows the cross section expected for the native conformation (crystal-structure coordinates).[28] This line was obtained from a least-squares fit to the data shown in Table 1, and it reflects the small change predicted to occur in the collision integral with temperature. At around room temperature the peak in the distribution is at a slightly smaller cross section than expected for the crystal structure, which indicates that the $(M + 5H)^{5+}$ charge state is slightly more compact in the gas phase than the crystal structure. As the temperature is raised, the peak in the distribution initially moves to slightly smaller cross sections, and then for temperatures above 423 K, the peak gradually moves to larger cross sections. The small initial decrease in the cross sections as the temperature is raised is approximately the same magnitude as the decrease in the collision integrals calculated for the native

(25) MacKerell, A. D.; Bashford, D.; Bellot, M.; Dunbrack, R. L.; Evanseck, J. D.; Field, M. J.; Fisher, S.; Gao, J.; Guo, H.; Ha, S.; Joseph-McCarthy, D.; Kuchnir, L.; Kuczera, K.; Lau, F. T. K.; Mattos, C.; Michnick, S.; Nago, T.; Nguyen, D. T.; Prodhom, B.; Reiher, W. E.; Roux, B.; Schlenkrich, M.; Smith, J. C.; Stote, R.; Straub, J.; Watanabe, M.; Wiòrkiewicz-Kuczera, J.; Yin, D.; Karplus, M. *J. Phys. Chem. B* **1998**, *102*, 3586.

(26) Mason, E. A.; McDaniel, E. W. *Transport Properties of Ions in Gases;* Wiley: New York, 1988.

(27) Mesleh, M. F.; Hunter, J. M.; Shvartsburg, A. A.; Schatz, G. C.; Jarrold, M. F. *J. Phys. Chem.* **1996**, *100*, 16082.

(28) Bushnell, G. W.; Louie, G. V.; Brayer, G. D. *J. Mol. Biol.* **1990**, *214*, 585.

(29) The Lennard−Jones parameters employed were $\epsilon_o = 0.65$ meV and $\sigma = 2.38$ Å for H−He interactions and $\epsilon_o = 1.34$ meV and $\sigma = 3.042$ Å for C−He and all other atoms. Here ϵ_o is the depth of the potential and σ is the distance where it passes through zero.

(30) Shvartsburg, A. A.; Jarrold, M. F. *Chem. Phys. Lett.* **1996**, *261*, 86.

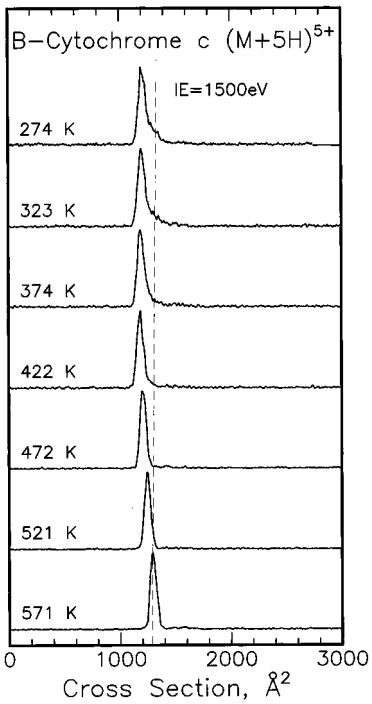

Figure 1. Cross-section distributions measured for the +5 charge state of bovine cytochrome *c* as a function of drift-tube temperature. The near-vertical dashed line is a least-squares fit to the collision integrals calculated for the crystal structure as a function of temperature using the trajectory model (see Table 1).

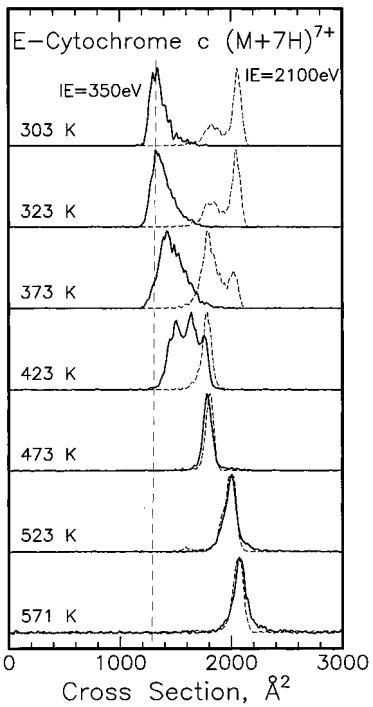

Figure 2. Cross-section distributions measured for the +7 charge state of equine cytochrome *c* as a function of drift-tube temperature. The solid lines show distributions measured with a low injection energy (350 eV), while the dashed lines show results obtained with a high injection energy (2100 eV). The near-vertical dashed line is a least-squares fit to the collision integrals, calculated for the crystal structure as a function of temperature using the trajectory model (see Table 1).

conformation using the classical trajectory model (the dashed line in the figure). The increase in the cross sections at higher temperatures indicates that the +5 charge state expands, slightly, above 423 K. The distributions shown in Figure 1 were recorded with a high injection energy, 1500 eV. However, the distributions for the $(M + 5H)^{5+}$ charge state do not change significantly when the injection energy is lowered. Mass spectra recorded with the drift tube at 573 K showed no evidence of the protein ions dissociating.

Unlike the $(M + 5H)^{5+}$ charge state, the distributions measured for the $(M + 6H)^{6+}$ and $(M + 7H)^{7+}$ charge states depend on the injection energy. At low injection energies, the ions retain a memory of their solution-phase structure,[31] and the distributions show a peak at cross sections close to that expected for the crystal structure. At high injection energies, the ions are heated and then cooled by collisions with the buffer gas. The peaks for the $(M + 6H)^{6+}$ and $(M + 7H)^{7+}$ charge states move to larger cross sections indicating that these charge states adopt partially unfolded conformations when they are collisionally heated.

Figure 2 shows distributions measured for the +7 charge state. The solid lines show the results for low injection energy, the dashed lines for high injection energy. At high injection energy, there are two peaks in the distribution measured at close to room temperature. As the temperature is raised to 423 K, the distribution shifts to the position of the room-temperature peak with the smaller cross section, and then for temperatures above 473 K, the peak moves back to larger cross sections. At low injection energy, the distribution measured at close to room temperature shows a broad peak close to the cross section for the crystal structure. As temperature is raised, the peak broadens and shifts to larger cross sections. At 423 K, three peaks are apparent, and then for 473 K and above a single peak is observed

(31) Hudgins, R. R.; Woenckhaus, J.; Jarrold, M. F. *Int. J. Mass Spectrom. Ion Processes* **1977**, *165/166*, 497.

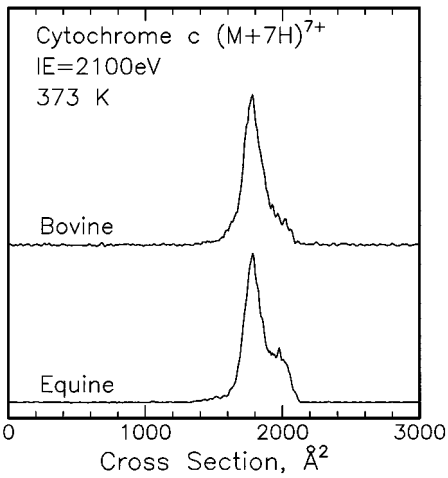

Figure 3. Comparison of the cross-section distributions measured for the +7 charge state of equine and bovine cytochrome *c* at high injection energy and with a drift-tube temperature of 373 K.

at the same position as the high-injection-energy peak. The behavior for the $(M + 6H)^{6+}$ charge state of equine cytochrome *c* is quite similar to that of the +7 charge state except that the +6 charge state does not unfold as much at the higher temperatures. Results for the +6 charge state are included in the Supporting Information.

The results shown in Figure 2 are for equine cytochrome *c*. Results obtained with bovine cytochrome *c* are almost identical. Bovine and equine cytochrome *c* differ by only two residues, so this similarity is not surprising. Despite this, we did observe a small but significant difference between the results for bovine and equine cytochrome *c*. Figure 3 shows distributions recorded for the $(M + 7H)^{7+}$ charge state at 373 K. The relative

abundance of the peak with the larger cross section is larger for equine cytochrome *c* than for bovine cytochrome *c*. In this temperature range, the peak at larger cross section is converting into the one with the smaller cross section. Thus, the substitutions in equine cytochrome *c* appear to stabilize the conformation with the larger cross section. This significant result demonstrates the possibility of performing directed substitutions to probe interactions within an unsolvated protein, an approach widely used in solution studies.

V. MD Simulations. Ab initio and semiempirical methods have been used to study small peptides,[32−36] but the dynamic nature of a protein like cytochrome *c* is best addressed by MD simulations using an empirical force field. While there have been many MD simulations of unsolvated neutral proteins, the first MD simulations for multiply charged proteins, specifically aimed at understanding gas-phase measurements, have only recently been reported (after this manuscript was submitted).[37] In this work, Reimann and collaborators examined the unfolding of highly charged lysozyme, though they did not perform a quantitative comparison with experimental results.

An issue that needs to be addressed before MD simulations can be performed for a large multiply charged protein ion is how the protons are distributed between the basic sites. In previous MD simulations of small singly charged peptides, the site with the highest proton affinity was usually protonated.[15,38] For a multiply charged protein there are many basic sites, and the potential energy of a given charge permutation includes contributions both from Coulomb repulsion between the protons and from self-solvation. It is impractical to attempt a direct calculation, incorporating structural relaxation, of the energies for all of the possible charge permutations. Schnier et al.[39] and Miteva et al.[40] have developed schemes to determine the lowest energy charge permutation by calculating electrostatic energies for the crystal structure. We used a similar approach to identify an ensemble of low-energy charge permutations starting with the crystal structure, and then relaxed their geometries, before selecting the lowest energy ones for MD simulations. Ideally, the possibility of proton-transfer processes should be incorporated into the MD simulations. However, the treatment of charge transfer within classical MD largely has been limited to small and simple systems.[41−44] In the work described here the protons are fixed to specific sites during the simulations.

V.A. Computational Details. We used the CHARMM force field[24,25] with the 21.3 parameter set. This force field was parametrized for proteins and peptides and includes van der Waals interactions, electrostatic interactions, and internal-energy terms. Hydrogen-bonding interactions, which are primarily electrostatic, are incorporated in the electrostatic terms. The internal-energy contribution to the force field results from distortion of chemical bonds from their most favorable conformations and includes terms for bond length, bond angle, dihedral angle, and improper torsions. To simulate gas-phase conditions, acidic and basic side chains were neutral, except for the basic residues that were protonated to provide the charge. The equations of motion were integrated with the Verlet algorithm,[45] and the bond lengths were constrained by the SHAKE method.[46] A time step of around 1 fs was used. CH, CH_2, and CH_3 groups were treated as extended atoms. The dielectric constant was taken as 1.0. In what follows we will refer to the total potential energy as the total energy; the kinetic energy will of course change during the MD simulations, but it is not relevant.

V.B. Location of the Protons. Since it is not possible to perform simulations for all of the charge permutations of cytochrome *c*, we used a simple procedure to identify a few of the low-energy ones. To make the problem more manageable, we only considered protonation of the 23 more basic Arg, His, and Lys residues. We calculated the total energies of all of the different charge permutations for the crystal structure using the CHARMM force field, and then added a term to account for the different intrinsic proton affinities of the protonated residues.[47] We subjected the 40 lowest energy ones to a crude energy minimization (1140 steps with a conjugate-gradient method). MD simulations were then performed for the low-energy charge permutations, as described in detail below. In addition to minimizing the 40 lowest energy permutations, we also minimized 40 medium-energy and 40 high-energy ones. The energies of the permutations from the high-, medium-, and low-energy regimes remained fairly distinct after optimization, which suggests that the first step in our procedure can be used as a pre-filter to select low-energy charge permutations for more detailed study.

For the +5 charge state the 10 lowest energy charge permutations after minimization were selected for MD simulations along with three others chosen to provide a sample of different permutations. For the +7 charge state, where many of the low-energy permutations were similar, we selected the five lowest energy ones plus seven more to provide variety. Simulations were generally run for 240 or 480 ps depending on how long it took to reach a steady state. Average cross sections and energies were derived from a further 15-ps simulation performed after the first 240 or 480 ps. Tables summarizing the results for the different +5 and +7 charge permutations at both 300 and 600 K are given in the Supporting Information. Table 2 shows values for the cross sections, radii of gyration, and the different energy terms obtained by averaging over the five lowest energy simulations for each charge state and temperature.

V.C. MD Simulation for Neutral Cytochrome *c*. A simulation was performed at 300 K for neutral cytochrome *c* for comparison with the simulations with different charge states. The starting point was the crystal structure, and the simulation was performed for 480 ps at 300 K. Figure 4 (top panels) shows a comparison of the crystal structure and a representative

(32) Head-Gordon, T.; Head-Gordon, M.; Frisch, M. J.; Brooks, C. L.; Pople, J. A. *J. Am. Chem. Soc.* **1991**, *113*, 5989.
(33) Zhang, K.; Zimmerman, D. M.; Chung-Phillips, A.; Cassady, C. J. *J. Am. Chem. Soc.* **1993**, *115*, 10812.
(34) Zhang, K.; Cassady, C. J.; Chung-Phillips, A. *J. Am. Chem. Soc.* **1994**, *116*, 11512.
(35) Cassady, C. J.; Carr, S. R.; Chung-Phillips, A. *J. Org. Chem.* **1995**, *60*, 1704.
(36) Wyttenbach, T., Bushnell, J. E.; Bowers, M. T. *J. Am. Chem. Soc.* **1998**, *120*, 5098.
(37) Reimann, C. T.; Velazquez, I.; Tapia, O. *J. Phys. Chem. B* **1998**, *102*, 9344.
(38) Blatt, H. D.; Smith, P. E.; Pettitt, B. M. *J. Phys. Chem. B* **1997**, *101*, 7628.
(39) Schnier, P. D.; Gross, D. S.; Williams, E. R. *J. Am. Chem. Soc.* **1995**, *117*, 6747.
(40) Miteva, M.; Demirev, P. A.; Karshikoff, A. D. *J. Phys. Chem. B* **1997**, *101*, 9645.
(41) Caldwell, J.; Dang, L. X.; Kollman, P. A. *J. Am. Chem. Soc.* **1990**, *112*, 9144.
(42) Dang, L. X.; Smith, D. E. *J. Chem. Phys.* **1993**, *99*, 6950.
(43) Lynden-Bell, R. M.; Rasaiah, J. C. *J. Chem. Phys.* **1997**, *107*, 1981.
(44) Alavi, A.; Alvarez, L. J.; Elliot, S. R.; McDonald, I. R. *Philos. Mag. B* **1992**, *65*, 489.
(45) Verlet, L. *Phys. Rev.* **1967**, *159*, 98.
(46) Van Gunsteren, W. F.; Berendsen, H. J. C. *Mol. Phys.* **1977**, *34*, 1311.
(47) The intrinsic-proton-affinity scale we employed is (in kJ mol^{-1}): Arg 1079, His 1039, Lys 1031, Gln 1016, Trp 1003, Pro 1003, and for all other (protonation of the backbone amide) 950. The scale was derived from the work of Williams and collaborators.[38]

Table 2. Overview of the MD Simulations for Neutral, the +5 Charge State, and the +7 Charge State of Equine Cytochrome *c* at 300 K and 600 K[a]

			energy, kJ mol^{-1}			
	cross section, Å^2	radius of gyration, Å	van der Waals	electrostatic	internal	total[b]
crystal structure	1339	12.6	−2209	−14 002	4478	−11 732
neutral at 300 K	1333	12.5	−2347	−15 690	3540	−14 498
average +5 at 300 K	1385	12.7	−1974	−16 467	3840	−14 654
average +7 at 300 K	1409	13.0	−1924	−16 132	3885	−14 261
average +5 at 600 K	1451	13.7	−1484	−15 989	5953	−11 570
average +7 at 600 K	1685	18.9	−1292	−15 756	5978	−11 142

[a] For the +5 and +7 charge states at 300 and 600 K the quantities are averaged over the five lowest energy simulations. [b] The total energy is the sum of the van der Waals, electrostatic, and internal energies, plus a term to account for the different proton affinities of protonated sites: $\sum (PA_{Lys} - PA_i)$ where PA_{Lys} is the intrinsic proton affinity of lysine and PA_i is the intrinsic proton affinity of the protonated residue.

structure from the MD simulation. There were no substantial structural changes during the simulation. Both the average radius of gyration (12.5 Å) and the average collision cross section (1333 Å^2) are similar to those calculated for the crystal structure (12.6 and 1339 Å^2).

V.D. MD Simulations for the +5 Charge State. Figure 5 shows a plot of the total potential energy and cross section for the first 240 ps for one of the +5 simulations at 300 K. The total energy takes around 150 ps to stabilize, during which time the energy decreases substantially while the cross section changes only slightly. Figure 4 (middle panel) shows representative structures from the two MD simulations with the lowest total energies. At 300 K the +5 charge state remains similar to the crystal structure. The average radius of gyration (12.7 Å) and average cross section (1385 Å^2) are both slightly larger than those obtained for the neutral protein (Table 2). The dispersion in the cross sections for the different charge permutations is relatively small, 1364−1418 Å^2. Inspection of the energy terms in Table 2 shows that the electrostatic energy is more negative for the +5 charge state than for the neutral protein. Coulomb repulsion between the five protons must be offset by hydrogen bonding, or intramolecular self-solvation, in which atoms with partial negative charges move toward the protons and atoms with partial positive charges move away. The decrease in the electrostatic energy is offset by the van der Waals energy becoming less negative and the internal energy becoming more positive.

In the native conformation, the heme iron is bound on opposite sides of the heme plane to a His18 nitrogen and a Met80 sulfur. The coordination of the iron plays an important role in maintaining the closed heme crevice of cytochrome *c*. When cytochrome *c* unfolds in solution, His18 remains coordinated to the heme iron, whereas Met80 is displaced by another ligand.[48] In the neutral protein, the heme group remained coordinated to the Met80 sulfur. However, for the +5 charge state at 300 K the Met80 ligand is replaced in all of the simulations by an oxygen atom from Thr67.[49]

The average cross section and radius of gyration (1451 Å^2 and 13.7 Å) for the five lowest energy +5 simulations at 600 K are around 10% larger than those obtained at 300 K (see Table 2). However, all the conformations retain a tertiary structure similar to the crystal structure. Most of the three large helices remain intact. Figure 4 (bottom panel) shows representative structures from the two +5 simulations at 600 K with the lowest total energies. Comparison of the results at 300 and 600 K (see Table 2) shows that the internal energy increases as the temperature is raised (because of the increase in the vibrational potential energy) while the electrostatic and van der Waals energies become less negative (presumably because the slight expansion of the protein weakens these interactions). The heme iron remains coordinated to the His18 nitrogen. The Met80 sulfur is usually replaced by an oxygen atom from either Thr67 or Thr78.

V.E. MD Simulations for the +7 Charge State. Typical structures from the two lowest energy simulations for the +7 charge state at 300 K are shown in Figure 6 (upper panel). At 300 K, all the +7 charge permutations stay compact. They all have a six-coordinate heme iron with an oxygen atom replacing the Met80 sulfur. While the +7 charge state retains most of the features of the crystal structure, it is further removed from the crystal structure than the +5 charge state. Comparison of average quantities for five lowest energy simulations for the +7 charge state at 300 K with similar averages for the +5 charge state (Table 2) shows that the addition of two extra protons causes the average electrostatic energy to become less negative. The average cross section increases slightly. This slight expansion is probably responsible for the average van der Waals energy becoming slightly less negative. In the simulations for the different charge permutations, the van der Waals energy is correlated with the cross section ($r^2 = 0.877$), while the electrostatic energy and total energy are not.

At 600 K, the +7 charge states are unfolded. The average cross section, 1685 Å^2, is significantly larger than the average at 300 K, 1409 Å^2. Figure 7 shows a plot of the total energy and cross section against time for one of the +7 simulations at 600 K. The cross section increases rapidly within the first 200 ps and then remains fairly constant. The large change in the cross section is not accompanied by a substantial change in the total energy. This is true for all the simulations performed for the +7 charge state at 600 K. The energies of the unfolded conformations are not that different from the energies of the folded ones. There is a large dispersion in the cross sections for the different charge permutations at this temperature (1554−2065 Å^2) which reflects the large range of different partially folded conformations present in the simulations. There is some correlation ($r^2 = 0.664$) between the cross sections and the van der Waals energy, but no correlation with the total energy. Compared with the +7 charge state at 300 K, at 600 K the average van der Waals energy and average electrostatic energy are both substantially less negative (see Table 2). Figure 6 (lower panels) shows two conformations from the +7 simulations at 600 K. At 600 K, the +7 charge state has lost essentially all remnants of its tertiary structure. However, the main secondary-structure features survive in most of the simulations. The bond between His18 and the heme iron persists, and there is a mixture of five-coordinate and six-coordinate iron with an oxygen ligand.

V.F. Self-Solvation of the Charge. Self-solvation has a significant effect on the structures and energies of multiply

(48) Pierce, M. M.; Nall, B. T. *Protein Sci.* **1997**, *6*, 618.

(49) In CHARMM the interactions around the Fe atom are electrostatic and van der Waals. There are no specific covalent interactions. This is similar to the view taken in crystal field theory.

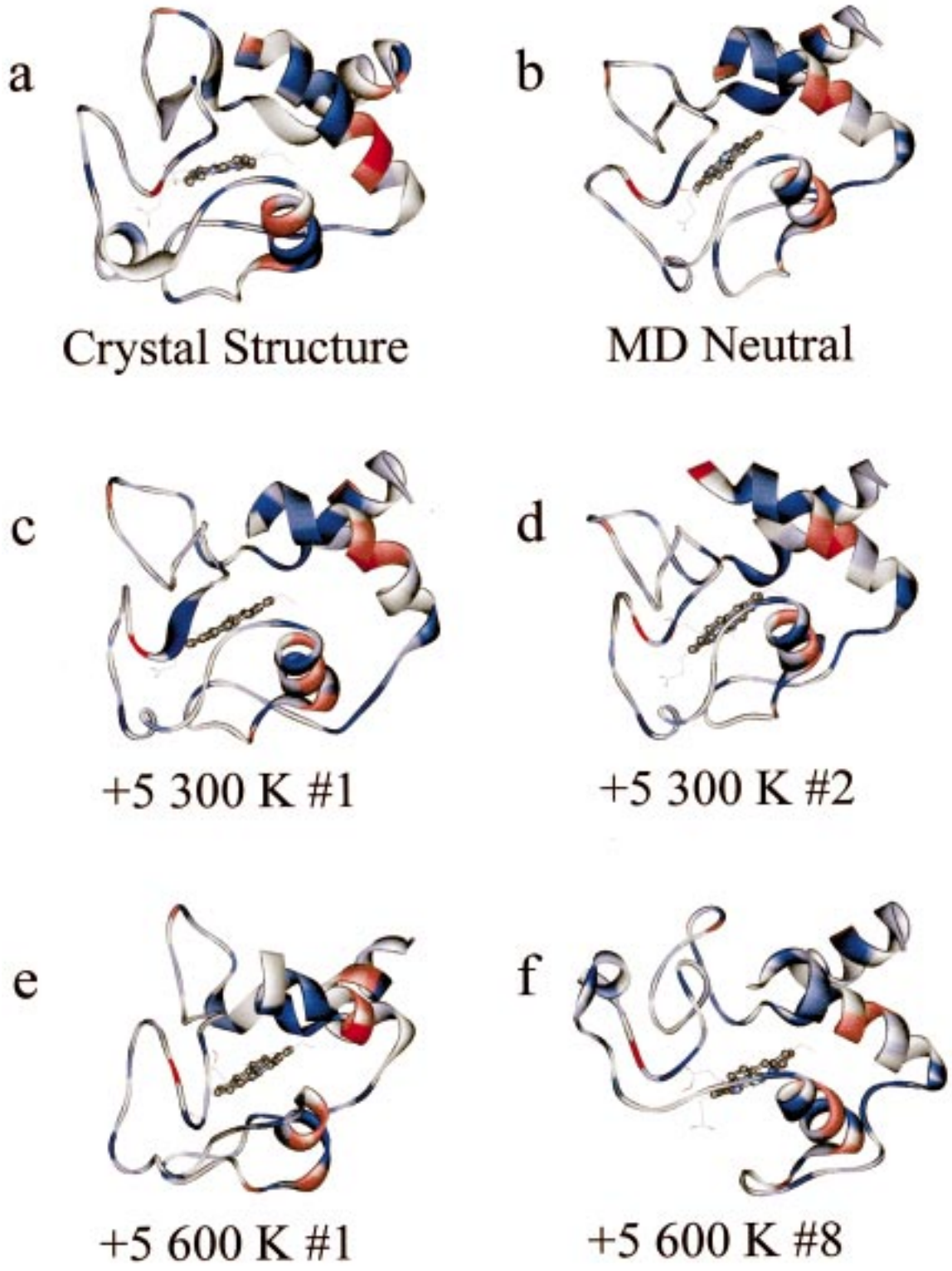

Figure 4. The crystal structure of equine cytochrome *c* (a) and a representative structure from the MD simulation for neutral cytochrome *c* (b). The middle panel shows representative structures for the two lowest energy simulations for the +5 charge state at 300 K. The structures shown are for charge permutations K13 K27 H33 K39 K55 (no. 1) (c) and K27 R38 K55 K73 K100 (no. 2) (d). The bottom panel shows representative structures from the two lowest energy MD simulations for the +5 charge state at 600 K. The structures shown are for charge permutations K13 K27 H33 K39 K55 (no. 1) (e) and K27 R38 K55 K72 R91 (no. 8) (f). The residues are colored on a gradient from red to white to blue for negative to positive hydrophobicity.

protonated protein ions; it is accomplished by the formation of hydrogen bonds between protonated groups and oxygen atoms either from backbone carbonyl groups or from side chains. This phenomena has been observed in MD simulations for small protonated peptides.[15] In the simulations of cytochrome *c*, the hydrogens and the oxygens both form more than one "hydrogen bond" even in the unfolded conformations. So it is better to describe the self-solvation in terms of a "solvation shell" formed by the oxygens rather than by the number of hydrogen bonds formed. The number of oxygens in the solvation shell depends

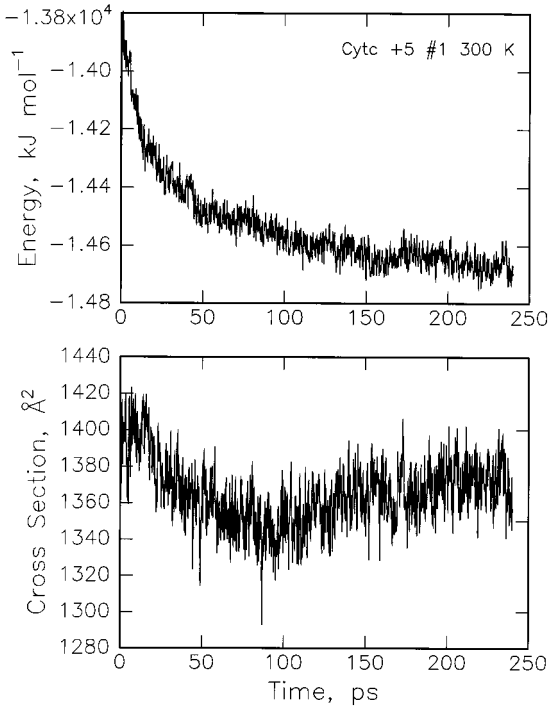

Figure 5. Plot of the total energy and cross section for the first 240 ps of the MD simulation for charge permutation K13 K27 H33 K39 K55 (the lowest energy simulation) for the +5 charge state at 300 K.

on the residue: for lysine there are three to six, with five being the most common; for arginine there are four to eight, with six being the most common; and for histidine there is only one or two. The size of the solvation shell is determined mainly by the number of hydrogen atoms that the charge is distributed over (four for arginine, three for lysine, and one for histidine). After the solvation shells form in the MD simulations they are relatively stable, and only small fluctuations occur during the rest of the simulation.

VI. Discussion

VI.A. Overview of the Experimental Results. The experimental results presented above show that the $(M + 5H)^{5+}$ charge state of cytochrome *c* remains compact as the temperature is raised to 573 K, while the $(M + 6H)^{6+}$ and $(M + 7H)^{7+}$ charge states unfold. In solution, where similar charge states exist, cytochrome *c* is denatured at much lower temperatures, below 353 K. The denaturation temperature depends on the solution conditions and decreases with decreasing pH[50] in much the same way as the denaturation temperature for the unsolvated protein decreases with increasing charge.

An unusual feature of the data measured for the +6 and +7 charge states with high injection energy is that the cross sections initially decrease as the temperature is raised. For example, at room temperature the +7 charge state shows two peaks (dashed line in Figure 2), and as the temperature is raised intensity shifts to the peak with the smaller cross section. We believe that this behavior results because in the high-injection-energy experiments the ions are rapidly cooled after they have been collisionally heated, freezing in higher temperature conformations.

McLafferty and collaborators have reported several studies of the conformations of gas-phase cytochrome *c* ions using H/D exchange.[4,5] They discuss several phenomena also seen in the current work, including the thermal/Coulomb denaturing and the importance of self-solvation. Some of their observations have been difficult to reconcile with our ion-mobility measurements, though both experiments indicate the presence of multiple conformations. In a recent paper, McLafferty et al. reported measurements for cytochrome *c* as a function of temperature.[5] For all of the charge states that were examined (+9 to +17) the H/D exchange levels were found to increase to a maximum at around 353−373 K and then decrease again. These results appear to suggest that cytochrome *c* ions unfold and then, at least partly, refold as the temperature is raised. However, the interpretation of H/D exchange levels for gas-phase proteins is not as straightforward as in solution.[51,52] Exposed basic hydrogens do not exchange efficiently in the gas phase unless they are near another basic residue because of the mechanism of the H/D exchange process. Changing the temperature may affect the number of exchangeable hydrogens without causing a gross conformational change like the unfolding transition studied in the present work.[53]

VI.B. Comparison of the Measured and Calculated Cross Sections at 300 K. The average cross sections calculated for the crystal structure and the neutral protein at 300 K are 1339 and 1333 Å^2, respectively (see Table 2). Therefore, no significant shrinkage occurs in the simulations on going from the crystal to the gas phase. In previous MD simulations for BPTI using an earlier force field, a decrease of 7.8% in the radius of gyration was reported.[54] This behavior was rationalized by suggesting that the crystal environment provides an effective force field that stops the protein from packing as tightly as possible. We performed MD simulations for uncharged BPTI and found that the radius of gyration decreased by around 2.4% compared to the crystal structure. So the CHARMM force field we employed leads to less shrinkage in a vacuum. The experimental results indicate that the shrinkage is a real phenomena. The measured cross sections for the +5 and +7 charge states at room temperature, around 1200 Å^2 and 1300 Å^2, respectively, are smaller than the cross section calculated for the crystal structure (1339 Å^2). The average cross sections calculated from the MD simulations for the +5 and +7 charge states, 1385 Å^2 and 1409 Å^2, respectively, are significantly larger than the measured ones. The discrepancy between calculated and measured cross sections suggests that the force field does not properly permit the protein to contract in the absence of a solvent or crystal environment, presumably because the short-ranged repulsions are too strong. The CHARMM force field, like most force fields used to study biomolecules, is really parametrized to match protein or peptide behaviors in the solution or crystalline phases. So this failure is perhaps not surprising. However, it suggests a significant shortcoming: if the solvent is not required to reverse the vacuum shrinkage, then both the intramolecular interactions and the protein−solvent interactions are deficient, even though the combination yields conformations in agreement with experiment.

VI.C. Comparison of the Measured and Calculated Cross Sections at 600 K. Measured cross sections for the +5 charge state increase from around 1200 Å^2 at room temperature to around 1300 Å^2 at 573 K. The calculated cross sections increase by slightly less, from 1385 to 1451 Å^2 (Table 2). For the +7 charge state, the increase in the cross section is larger because this charge state unfolds. The measured cross sections increase

(50) Privalov, P. L.; Kechinashvili, N. N. *J. Mol. Biol.* **1974**, *86*, 665.

(51) Campbell, S.; Rodgers, M. T.; Marzluff, E. M.; Beauchamp, J. L. *J. Am. Chem. Soc.* **1995**, *117*, 12840.

(52) Wyttenbach, T.; Bowers, M. T. *J. Am. Soc. Mass Spectrom.* **1999**, *10*, 9.

(53) Valentine, S. J.; Liu, Y.; Clemmer, D. E., to be published.

(54) Van Gunsteren, W. F.; Karplus, M. *Biochemistry* **1982**, *21*, 2259.

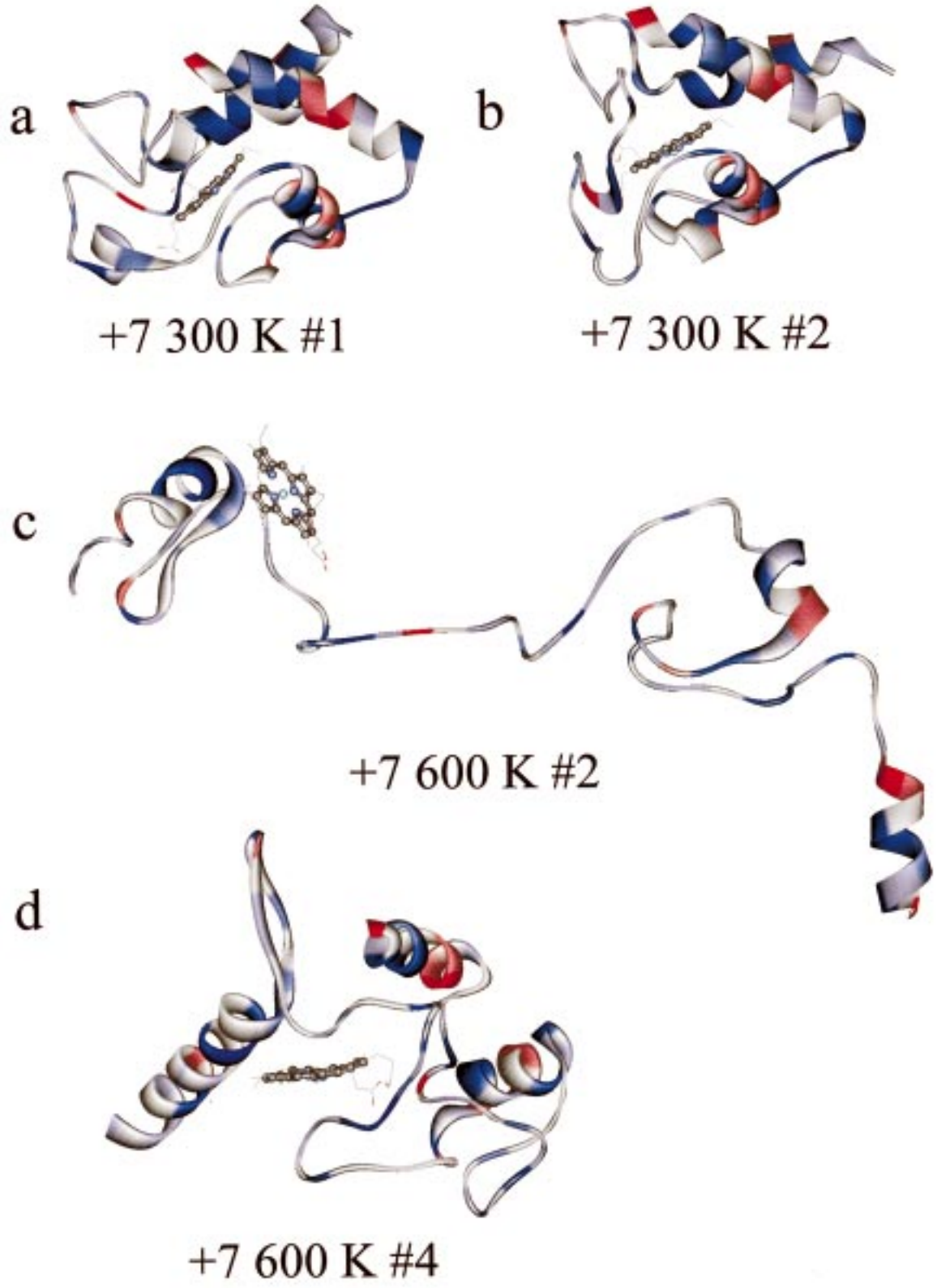

Figure 6. Representative structures from the simulations for the +7 charge state. The upper panel shows structures from the two lowest energy simulations at 300 K. The structures shown are for charge permutations K13 K27 R38 K55 K72 R91 K100 (no. 1) (a) and K13 K27 R38 K55 K79 R91 K100 (no. 2) (b). The lower panel shows representative structures for the +7 charge state at 600 K. The structures shown are from the lowest energy simulation K13 K27 R38 K39 K55 R91 K100 (no. 4) (d) (computed cross section 1554 Å^2) and from the one with the largest cross section (2065 Å^2) K13 K27 R38 K55 K79 R91 K100 (no. 2) (c). The residues are colored on a gradient from red to white to blue for negative to positive hydrophobicity.

from around 1300 Å^2 to around 2000 Å^2. The calculated cross sections increase from 1409 to 1685 Å^2 at 600 K. This increase is significantly smaller than that observed in the experiments. There are several possible reasons for this discrepancy (even beyond the quantitative inadequacy of the CHARMM force field). First, the time scales of the measurements and simulations

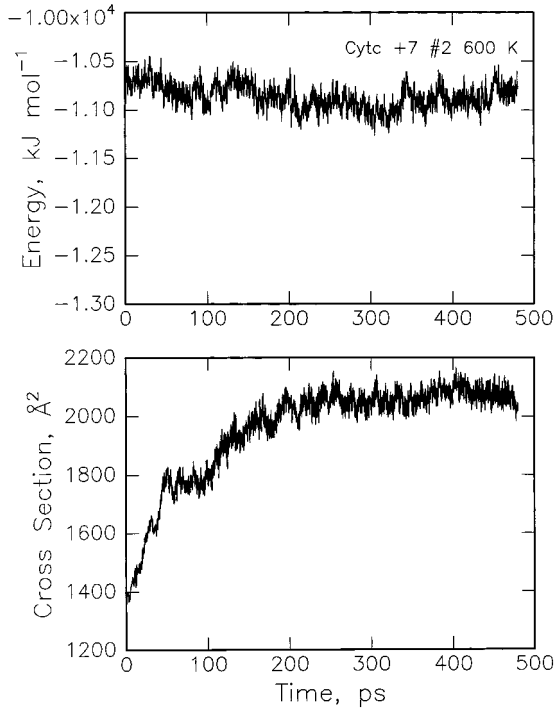

Figure 7. Plot of the total energy and cross section against time for charge permutation K13 K27 R38 K55 K79 R91 K100 for the +7 charge state at 600 K.

are very different. If the simulations were run for microseconds, instead of a fraction of a nanosecond, further unfolding of the +7 charge state may occur at the higher temperature. Second, the average values quoted above were for the five lowest energy simulations at each temperature. There is a wide dispersion in the cross sections for the +7 charge state at the higher temperature (1554−2065 Å^2), and it is possible that the charge permutations sampled in the experiments have the larger cross sections.

It is important to note that the major qualitative difference in the experimental cross sections is well described by the simulations. For the +5 charge state, the cross-section increase in the simulations is small as the temperature is raised, because most of the tertiary structure remains intact (Figure 4), while for the +7 charge state several important tertiary-structure features disappear as the protein is heated to 600 K (Figure 6), and the average cross section increases significantly. The broad dispersion in the cross sections for the +7 charge state at 600 K indicates that the location of the charge has a strong influence on the details of the unfolding process, with different charge permutations following different unfolding trajectories. This is mirrored in the experimental results, where the peak widths for the +5 at all temperatures are narrower than those for the +7 at 573 K.

VI.D. The Role of Coulomb Repulsion. With the addition of five or seven protons to cytochrome *c*, the electrostatic energy becomes more negative than that for the neutral protein (see Table 2) because the favorable effects of self-solvation overcome the unfavorable effects of Coulomb repulsion. However, the charge causes the protein to expand, causing the van der Waals energy to become less negative. The internal energy also increases as the protein becomes less compact. The net result is that the total energies of the neutral protein and the +5 charge state are similar. With the addition of two more protons to give the +7 charge state, the electrostatic energy becomes more positive as Coulomb repulsion now outweighs self-solvation, and the total energy becomes less negative. It has been argued that in solution at neutral pH charge−charge interactions stabilize the folded conformation; while at low pH, further ionization is destabilizing.[55] The behavior in the gas phase appears to parallel that in solution.

Coulomb repulsion between the protons must decrease when the protein unfolds; however, comparison of the results in Table 2 for both charge states and both temperatures suggests that the change in Coulomb repulsion is more than offset by the loss of favorable electrostatic attractions. The change is greater for the +5 than the +7. On comparing the differences between the +5 at the two differing temperatures and the +7 at those same temperatures, we see that the electrostatic energy apparently becomes slightly (∼100 kJ mol^{-1}) more negative upon unfolding. This change in the electrostatic energies is compensated by a loss of van der Waals interactions as the protein unfolds (see Table 2), so that the overall energy change is close to zero. (That is, the total energy change on going from the 300 to the 600 K structure is nearly identical for the +5 and the +7.) While increasing the charge does cause the protein to unfold, the view that it destabilizes the protein through Coulomb repulsion is obviously an oversimplification.

The delicate balance between the different energy terms is demonstrated by Figure 7, which shows the total energy and cross sections during the unfolding of one of the +7 charge states. The cross section increases dramatically as the protein unfolds, but the total energy hardly changes. This behavior is strikingly different from that shown in Figure 5, where the +5 ion undergoes changes that lower the energy but leave the cross section roughly constant. These results show that the relevant configuration space for the +7 charge state is "flatter" than that for the +5, so that the folding "funnels"[56] will be less dominant and entropy effects more important. The deep folding funnel for the +5 charge state traps the protein, even as the temperature is raised to 573 K, while for the +7 charge state the flatter free-energy landscape means that unfolding can occur in a facile manner when the temperature is raised. Entropy, which is implicitly included in a molecular dynamics simulation, presumably drives the unfolding of the +7 charge state as the temperature is raised.

VI.E. Separation of the Terminal Helices. In the simulations at 300 K, the +5 and +7 states are similar to the crystal structure. Even the +5 charge state at 600 K still retains some of the major features of the crystal structure. In particular, the two terminal helices have not separated. The interaction between the terminal helices is a highly conserved tertiary-structure interaction in cytochrome *c*. Pairing of these helices is one of the earliest detectable structural events in the folding of cytochrome *c*.[57] A major difference between the +5 and +7 states at 600 K is that the terminal helices have separated for the +7 state (compare Figures 4 and 6). However, separation of the terminal helices does not always lead to unfolding. For structure d of Figure 6, the helices have separated, but the protein has not really unfolded.

VII. Conclusions

The thermal unfolding of unsolvated cytochrome *c* has been examined using ion-mobility measurements and MD simula-

(55) Yang, A.; Honig, B. *Biochemistry* **1993**, *21*, 2259.

(56) Bryngelson, J. D.; Onuchic, J.; Socci, N. D.; Wolynes, P. G. Proteins: Struct., Funct., Genet. **1995**, *21*, 167−195. Wolynes, P. G. *Proc. Natl. Acad. Sci. U.S.A.* **1995**, *93*, 2426.

(57) Roder, H.; Elöve, G. A. In *Mechanism of Protein Folding: Frontiers in Molecular Biology*; Pain, R. H., Ed.; Oxford University Press: New York, 1994.

tions. In the experiments, the +5 charge state remains folded at 573 K, while the +6 and +7 charge states go through a series of unfolding transitions as the temperature is raised. Cross sections determined from MD simulations for the +5 and +7 charge states at 300 K are significantly larger than those observed in the experiments. This is almost certainly due to an inadequate treatment of short-range repulsions in the CHARMM[24,25] force field. The MD results nevertheless provide important insight into the experimental results. One reason for this utility is the essential insensitivity of the unfolding (and other biophysical phenomena) to minor details; even extensive homology differences often do not change major biophysical or functional properties of proteins, partly because such major changes as unfolding are statistically favored for the overall ensemble or population.

Probably the most significant and striking observation seen in the experiments is both reproduced and illuminated by the MD simulations: the cross section for the +5 charge state increases only slightly on going from ambient temperature to 573 K, while the cross section for the +7 charge state increases significantly. These behaviors are reproduced by the MD simulations, which show much larger changes on heating the +7 than on heating the +5 (although the absolute differences seen experimentally are not reproduced in the simulations, as a result both of force field inadequacy and of limited sampling). The simulations provide insight into the compensating effects of Coulomb repulsion and self-solvation, the role of the terminal helix contact in the unfolding process, and the nature of the free-energy landscape, which is much more flat for the +7 charge state than for the +5.

Acknowledgment. The experiments were performed on an apparatus supported by the National Science Foundation (CHE-9618643). The donors of the Petroleum Research Fund, administered by the American Chemical Society, are acknowledged for partial support of this work. M.R. thanks the Chemistry Division of NSF and the DOE/LBL Advanced Batteries Program for support. We are grateful to Professors F. W. McLafferty and M. T. Bowers for helpful comments.

Supporting Information Available: We present a figure showing cross-section distributions for the +6 charge state of cytochrome *c* as a function of temperature and four tables which summarize the results of the MD simulations performed on the different charge permutations. In the tables we show results for the ten lowest energy simulations. The quantities in the tables were obtained from a 15-ps simulation after the system had reached a steady state in either a 240-ps or a 480-ps simulation. This material is available free of charge via the Internet at http://pubs.acs.org.

JA980324B